Breathers in strongly anharmonic lattices

Philip Rosenau
School of Mathematics, Tel-Aviv University, Tel-Aviv 69978, Israel

Arkady Pikovsky
Institute for Physics and Astronomy, University of Potsdam, 14476 Potsdam, Germany

(Received 21 August 2013; revised manuscript received 2 January 2014; published 26 February 2014)

We present and study a family of finite amplitude breathers on a genuinely anharmonic Klein-Gordon lattice embedded in a nonlinear site potential. The direct numerical simulations are supported by *a quasilinear Schrodinger equation* (QLS) derived by averaging out the fast oscillations assuming small, albeit finite, amplitude vibrations. The genuinely anharmonic interlattice forces induce breathers which are strongly localized with tails evanescing at a doubly exponential rate and are either close to a continuum, with discrete effects being suppressed, or close to an anticontinuum state, with discrete effects being enhanced. Whereas the D-QLS breathers appear to be always stable, in general there is a stability threshold which improves with spareness of the lattice.

DOI: 10.1103/PhysRevE.89.022924 PACS number(s): 05.45.−a, 63.20.Pw, 63.20.Ry

I. INTRODUCTION

Since their introduction over two decades ago by Sievers and Takeno, the intrinsically localized modes (ILMs), or breathers, of the lattice have found a wide range of applications; see Refs. [1–4], and references therein. Their formation is due to competing elements; discreteness and nonlinearity either due to interparticles interaction or due to the nonlinear site potential with the interaction between adjacent elements assumed to be linear. A large variety of such ILMs was found, characterized by a finite number of nodal points (masses in the Newtonian case) being strongly excited, with typical tails decaying exponentially. Typically these are microscopic modes with discreteness of the lattice playing an essential role, and they do not extend to the continuum level. In contradistinction, with one exception, the modes studied in the present paper have a finite macroscopic span which may depend on the amplitude but to a far lesser extent on the distance between the excited node points, and they naturally extend into the continuum. In fact, we shall use both the continuum and the anticontinuum limits to study the emerging structures in lattices with a nonlinear on-site potential and purely nonlinear intersite coupling (cf. Ref. [5]). A particular setup of this problem was studied by one of us in Ref. [6] where both the site potential and the interparticle interaction were assumed to be quartic (cf. Refs. [7–12]). Though more limited in scope, such a model has a great appeal because the resulting equations of motion on both discrete and continuum levels are space-time separable, which makes their dynamics accessible analytically and reveals large amplitude breathers of an almost compact span that vibrate at an anharmonic pace and stay indefinitely.

For other interaction potentials the miracle of separability is in general lost, and the resulting Klein-Gordon equation presents a formidable mathematical difficulty. It is thus natural that we first direct our attention to small, albeit finite, amplitude excitations, which enables us to average over a fast temporal oscillations and to derive on both the continuum and discrete levels a quasilinear Schrödinger equation (cf. Refs. [6,13]), which shall be referred to as a QLS and D-QLS equation, respectively. Both describe the slow vibrations of small amplitude breathers due to a wide variety of genuinely anharmonic interactions and site potentials.

When addressing large vibrations or testing the viability of the QLS model we have to address the original, genuinely anharmonic, Klein-Gordon lattice. But now since, unlike the QLS, the continuum rendition offers very little reprieve, it is natural to start at the opposite, anticontinuum, limit wherein the spatial separation ℓ diverges $1/\ell \downarrow 0$. Surprisingly enough, in this regime the strong anharmonicity acts in our favor; not only do the more robust breathers reside on sparse lattices, but this localizes the dynamics to the extent that it is confined to a very small number of mass points with the residents of the tail decaying at a doubly exponential rate and thus very quickly become exceedingly small.

II. LATTICES AND THEIR CONTINUUM LIMIT

We start with the Hamiltonian

$$H = \ell \sum_n \left\{ \frac{\dot{y}_n^2}{2} + P\left(\frac{y_{n+1} - y_n}{\ell} \right) + \Phi(y_n) \right\}, \qquad (1)$$

describing a chain of particles of equal masses (which is set to one) and equal spatial separation ℓ, where P and Φ denote the interaction and site potentials, respectively. We assume both potentials to be of a polynomial form

$$P(S) = \frac{a_p}{p+1}|S|^{p+1} \quad \text{and} \quad \Phi(y) = \frac{1}{2}y^2 - \frac{b_m}{m+1}|y|^{m+1}, \qquad (2)$$

with $p,m > 1$. For now we consider only the case of soft nonlinearity, $b_m > 0$, where the frequency of on-site oscillations decreases with the amplitude. The case of the hard nonlinearity $b_m < 0$ will be addressed later (see Sec. IV B). In realistic setups, the potential $\Phi(y)$ as in (2) should be considered as a low-amplitude rendition (so that one remains in the domain of bounded oscillations only) of a more general potential. Thus the standard potential $\sim 1 - \cos y$ corresponds to (2) with $m = 3$ and $b_m = 1/6$.

The essential superlinearity of the interparticle coupling, $p > 1$, makes the lattice genuinely anharmonic because linear

waves (phonons) do not exist. This necessitates a very different analysis from the one applicable to conventional breathers on lattices. We normalize the equations of motion due to the Hamiltonian (1): rescaling y one can set $b_m = 1$, whereas the constant a_p is absorbed in ℓ. We thus obtain a genuinely anharmonic Klein-Gordon lattice

$$\ddot{y}_n + y_n = \frac{1}{\ell}\left[\left(\frac{y_{n+1}-y_n}{\ell}\right)\left|\frac{y_{n+1}-y_n}{\ell}\right|^{p-1} - \left(\frac{y_n - y_{n-1}}{\ell}\right)\left|\frac{y_n - y_{n-1}}{\ell}\right|^{p-1}\right] + y_n|y_n|^{m-1}. \tag{3}$$

The continuum limit of the lattice model (3) when $\ell \to 0$ begets a quasilinear extension of the Klein-Gordon equation (QLKG),

$$y_{tt} + y = \frac{\partial}{\partial x}(y_x|y_x|^{p-1}) + y|y|^{m-1}. \tag{4}$$

We shall thus refer to its discrete antecedent, Eq. (3), as the D-QLKG equation. Note that the nonlinear force due to the anharmonic interactions constitutes a fundamental change, for unlike the conventional Klein/sine-Gordon semilinear scenarios, Eq. (4) is quasilinear. In general, in such equations second derivatives of solutions may blow up in a finite time (the mollifying effect of dispersion due to a site potential is in general ineffective in arresting the gradient catastrophe). It is the dispersion due to the discrete lattice which may prevent the blow up, *hence its singular effect on the dynamics*. In the small amplitude regime, Klein-Gordon equation can be simplified by virtue of the standard averaging procedure [14]. This is done by writing Eqs. (3) and (4) in terms of $w = Ke^{it}(y + iy_t)$, where K is a constant to be specified shortly. Dropping all terms containing an explicit time dependence it begets a quasilinear extension of the celebrated semilinear NLS equation in both discrete,

$$i\frac{dw_n}{dt} + K^{1-p}C_p\frac{1}{\ell}\left[\left(\frac{w_{n+1}-w_n}{\ell}\right)\left|\frac{w_{n+1}-w_n}{\ell}\right|^{p-1} - \left(\frac{w_n - w_{n-1}}{\ell}\right)\left|\frac{w_n - w_{n-1}}{\ell}\right|^{p-1}\right] + K^{1-m}C_m|w_n|^{m-1}w_n = 0\,, \tag{5}$$

where $C_p = \frac{\Gamma(p/2+1)}{\sqrt{\pi}\Gamma(p/2+3/2)}$, and continuous setups,

$$iw_t + K^{1-p}C_p\frac{\partial}{\partial x}[w_x|w_x|^{p-1}] + K^{1-m}C_m|w|^{m-1}w = 0.$$

Setting $K = (C_m/C_p)^{\frac{1}{m-p}}$ and $t \to tK^{p-1}/C_p$ we have

$$iw_t + \frac{\partial}{\partial x}[w_x|w_x|^{p-1}] + |w|^{m-1}w = 0. \tag{6}$$

We shall refer to Eqs. (5) and (6) as a discrete quasilinear Schrodinger (D-QLS) and a quasilinear Schrodinger (QLS) equation, respectively.

Equations (3)–(6) are a starting point of our search of time-periodic breathers which are spatially localized.

III. BREATHERS IN A CONTINUUM LIMIT

A. A distinguished $m = p$ case

In the distinguished case Eq. (4) admits separable $y = \phi(t)U(x)$ [6,15] solutions. We thus obtain a system

$$\ddot{\phi} + \phi = \lambda\phi|\phi|^{p-1}, \tag{7}$$

$$[U'|U'|^{p-1}]' + U|U|^{p-1} = \lambda U. \tag{8}$$

Equation (7) shows that below the critical amplitude the solution y is periodic in time, whereas above it blows up. For compactly supported solutions U has to vanish at a finite point. Such U, not vanishing identically, has a nonzero spatial extremum, at which $U' = 0$, thus $\lambda > 0$ for U to remain real when $U \sim 0$. The separation constant λ may then be eliminated rescaling ϕ and U leaving their product y unchanged. Integrating once we obtain

$$p|U'|^{p+1} + |U|^{p+1} = \frac{1+p}{2}U^2, \tag{9}$$

with integration constant discarded to ensure a compact solution. Equation (9) may be easily solved. In particular, for $p = m = 3$, [6], a breather's profile is given as

$$|x| = \frac{3^{1/4}}{2}\left[\sqrt{2}\pi - B\left(\frac{U^2}{2}, \frac{1}{4}, \frac{3}{4}\right)\right], \tag{10}$$

where B is the incomplete beta function. For this case, near the edge located at $x = L_3^3 \approx 2.92$ [see Eq. (14)] U vanishes and $U \sim \frac{(x-L_3^3)^2}{2\sqrt{6}}$, which causes Eq. (8) to degenerate there. The degeneracy enables to extend the solution by zero for $|x| > L_3^3$, yielding a strictly compact solution.

B. The general $m \neq p$ case

Whereas separation of variables is lost for the original Klein-Gordon setup, it still holds for the averaged small amplitude version (6). In fact, let $w = \exp(i\omega t)U(x)$ in (6) and integrating it once

$$\frac{2p}{p+1}|U'|^{p+1} + \frac{2}{m+1}|U|^{m+1} = \omega U^2\,, \tag{11}$$

where integration constant was discarded to ensure solitary solutions. Similarly to Eq. (8), Eq. (11) may also be integrated. To show the compact span of its solutions it suffices to observe that for $U \ll 1$; $|U'|^{p+1} \sim U^2$. Thus $U \sim (x - L_m^p)^{\frac{p+1}{p-1}}$ near the edge located at L_m^p, which is given via

$$L_m^p = \left(\frac{1+m}{1+p}p\right)^{\frac{1}{p+1}} U_m^{\frac{p-m}{p+1}}\mathbf{I}_m^p, \tag{12}$$

where $U_m = (\frac{m+1}{2}\omega)^{\frac{1}{m-1}}$ is the breather's height,

$$\mathbf{I}_m^p = \int_0^1 \frac{dz}{[z^2(1-z^{m_1})]^{\frac{1}{p+1}}} = \frac{1}{m_1}B\left(\frac{p}{p+1}, \frac{p-1}{m_1(p+1)}\right), \tag{13}$$

where $m_1 = m - 1$, and $B(x,y)$ is the beta function. In particular, when $m = p$, breathers' width

$$L_p^p = \frac{\pi p^{\frac{1}{p+1}}}{(p-1)\sin\left(\frac{\pi}{p+1}\right)} \tag{14}$$

is unaffected by changes in the breathers' oscillation frequency ω and thus in the amplitude. However, in general, changes in ω affect breathers' width with $m > p$ and $m < p$ cases reacting in an opposite manner; for $p > m$ taller breathers widen, whereas for $m > p$ they narrow. Note that similarly to the edge, smoothness near a breather's top depends on the value of p but not of m; $U \sim U_m(1 - \beta|x|^{\frac{1+p}{p}})$, $\beta = \text{const}$.

IV. BREATHERS ON LATTICES

A. Profiles

Again, we start with the distinguished $m = p$ case (though discussed in Ref. [6], we repeat it for completeness). The symmetry underlying the space-time separation remains intact in the discrete case (3) as well, and the ansatz $y_n(t) = \phi(t)Y_n$ results in Eq. (7) for the temporal part, whereas the spatial part begets a difference equation

$$\lambda Y_n = \frac{1}{\ell}\left[\left(\frac{Y_{n+1}-Y_n}{\ell}\right)\left|\frac{Y_{n+1}-Y_n}{\ell}\right|^{p-1} - \left(\frac{Y_n - Y_{n-1}}{\ell}\right)\left|\frac{Y_n - Y_{n-1}}{\ell}\right|^{p-1}\right] + Y_n|Y_n|^{p-1}. \tag{15}$$

The constant λ can again be set to one. Equation (15) has to be addressed numerically using, for instance, a shooting method. Separation of temporal and spatial dynamics implies that the form of the breather is independent of its period (and, correspondingly, its amplitude) and is solely determined by the spareness parameter ℓ. The results, together with all $m \neq p$ choices to be discussed shortly, are grouped together in Fig. 3.

Lifting the $m = p$ limitation, we start with the D-QLS [Eq. (5)] and utilize the separation of variables $w_n(t) = e^{i\omega t}U_n$, which holds for any m and p for the discrete version as well, and yields a finite difference system

$$K^{1-p}C_p\frac{1}{\ell^{1+p}}[(U_{n+1}-U_n)|U_{n+1}-U_n|^{p-1} - (U_n - U_{n-1})|U_n - U_{n-1}|^{p-1}] + K^{1-m}C_m U_n|U_n|^{m-1} = \omega U_n. \tag{16}$$

The freedom to choose K is now used again, and for $m \neq p$ we define

$$K = (\ell^{1+p}C_m/C_p)^{\frac{1}{m-p}}$$

[compare with the definition for the continuous case (6)] leaving the rescaled frequency $\Omega = \omega K^{p-1}/C_p$ as the only free parameter:

$$(U_{n+1}-U_n)|U_{n+1}-U_n|^{p-1} - (U_n - U_{n-1})|U_n - U_{n-1}|^{p-1} + U_n|U_n|^{m-1} = \Omega U_n. \tag{17}$$

For every Ω a localized solution of Eq. (17) can be found by shooting, with the amplitude U_0 being an adjustable free parameter. The properties of the resulting breathers are displayed in Fig. 1.

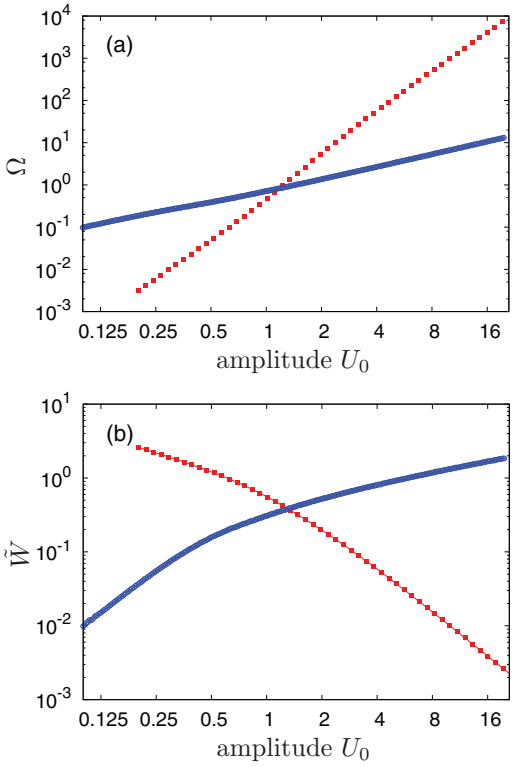

FIG. 1. (Color online) Breathers in lattice (17). (a) Dependence of the frequency Ω on the amplitude; (b) dependence of breathers' width, defined as $\tilde{W} = \frac{\sum_{n\geq 0} nU_n}{\sum_{n\geq 0} U_n}$, on the amplitude. Squares (red): $m = 4, p = 2$; circles (blue): $m = 2, p = 4$.

Returning to the original D-QLKG equation, unless $m = p$, to find breathers we have to resort to numerical means based on advancing from the anticontinuum, $1/\ell \to 0$, limit toward milder values of ℓ. In the "anti-" limit the coupling in (3) vanishes, and we have an entire range of on-site periodic orbits with corresponding different amplitudes. Pick one such solution, fix the resulting period, and follow it; take a small step in ℓ and march on. At each step, corresponding to a specific value of ℓ, use the available solution and apply Newton iterations to determine the subsequent breather having the same period. Reapplying this procedure one finds a sequence of periodic breathers of the D-QLKG lattice (3). Figure 2 displays samples of such breathers.

We use a sequence of breathers' periods to show in Fig. 3 the dependence of breathers' amplitude Y_0 and its width W, defined as $W = \ell\frac{\sum_{n\geq 0} nY_n}{\sum_{n\geq 0} Y_n}$, on the spareness parameter ℓ. One observes that the dependence of the amplitude on the spareness is basically the same irrespective whether $m > p$ or $m < p$, and, as expected, in the continuum $\ell \to 0$ limit breathers' amplitude is larger than in the anticontinuous, $1/\ell \to 0$, end. Larger amplitude always corresponds to a breather with a larger period (which, in fact, is determined by the sign of nonlinearity but not by its power). The dependence of breathers' width on ℓ is also qualitatively the same, with the extremal value attained in the continuum limit. However,

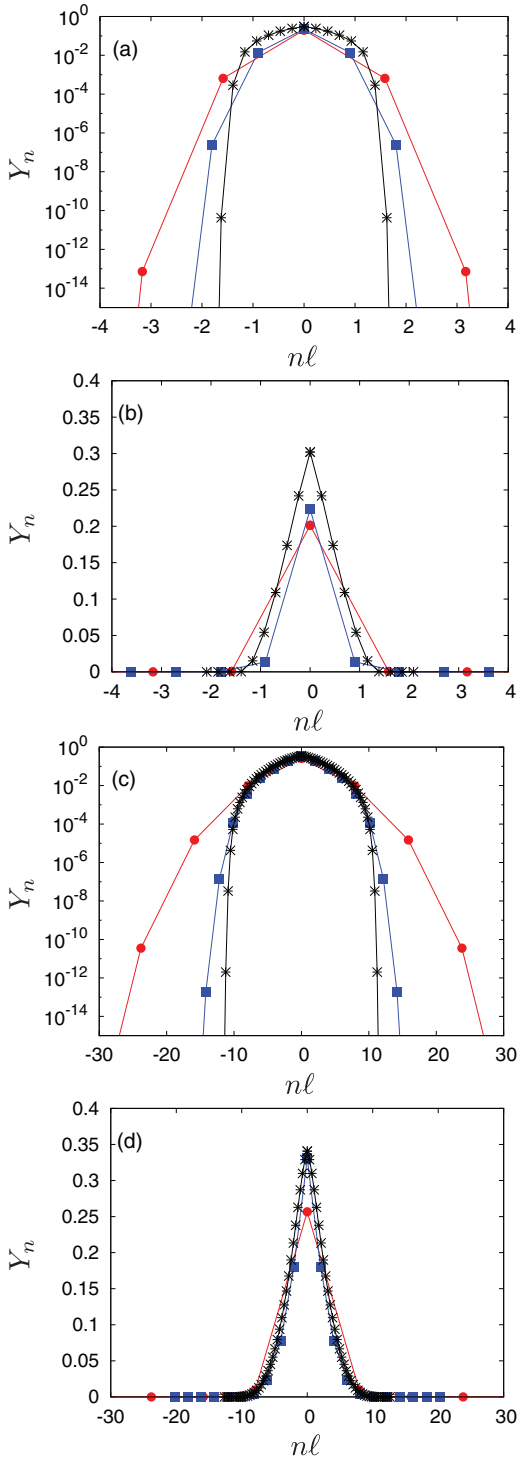

FIG. 2. (Color online) (a, b) $m = 2, p = 4$ (logarithmic and linear scale). Examples of breathers: $T = 6.8978$, $\ell = 1.5848935$ (red circles), $\ell = 0.9021607$ (blue squares), $\ell = 0.2319061$ (black asterisks). (c, d) $m = 4, p = 2$ (logarithmic and linear scale). Examples of breathers: $T = 6.3170$ $\ell = 7.937005$ (red circles), $\ell = 2.026838$ (blue squares), $\ell = 0.3506743$ (black asterisks).

breathers' width-amplitude relations are opposite: while for a given value of ℓ, $m > p$ breathers narrow with amplitude, for $m < p$ large-amplitude breathers widen. Notice that in the separable $m = p$ case the W vs ℓ dependence is the same for all periods and in plots like in Figs. 3(b) and 3(d) the different curves coalesce into the same line.

It is instructive to compare the D-QLKG breathers with their small amplitude separable offsprings, compliments of the corresponding D-QLS equation. This is accomplished via the scaling transformation that follows from (5) and (6):

$$\Omega' = \frac{T - 2\pi}{T C_m^{\frac{p-1}{p-m}} C_p^{\frac{m-1}{m-p}} \ell^{\frac{(m-1)(p+1)}{p-m}}},$$
$$U_0' = C_m^{1/(m-p)} C_p^{1/(p-m)} \ell^{\frac{p+1}{m-p}} Y_0. \tag{18}$$

In the scaled coordinates the data of Figs. 3(b) and 3(d) are replotted in Fig. 4 and compared with the predictions of the D-QLS displayed in Fig. 1(b). Similarly, we use the data of Figs. 3(a) and 3(c), apply the scaling (18), and in Fig. 5 compare it with the corresponding predictions of the D-QLS, shown in Fig. 1(a). Note the nearly perfect validity of the scaling as even at large amplitudes the breathers of D-QLS remain quite close to those of the D-QLKG.

Although empirically we observe a close affinity between the D-QLKG and the D-QLS breathers, nonetheless there is an fundamental difference between the two equations, for whereas the D-QLS admits separation of variables, unless $m = p$, the D-QLKG does not. It is thus of interest to look further into this issue. To test the separability feature we depict in Fig. 6 the evolution of the central site vs the evolution of site next to it. A straight line (but not ellipses) would indicate that there is no phase shift between the two sites, thus implying that the breather oscillates in-phase and thus space-time separability. However, the observed curves are not straight lines, say, $y_n(t) = \text{const} \cdot y_0(t)$. To quantify the deviation from separability we plot $[y_1 - \text{const} \cdot y_0(t)]$ vs $y_0(t)$. Though the deviations grow with breathers' amplitude, they remain quite small confirming quantitatively our observation that for a variety of m and p the dynamics of the D-QLKG lattice stays close to space-time separable conditions.

B. Three-points model

Unless resorting to head-on numerics, in the general nonseparable cases there is not much we can say about the dynamics of the original system in its continuous PDE rendition. Fortunately, whereas in the small amplitude regime the QLS suffices to describe both the structure and the dynamics of breathers, in the full problem the key to our understanding is found in the opposite, anticontinuum, regime where due to the very quick change of $\varepsilon = 1/\ell^{p+1}$ with ℓ, if $\ell < 1$ we are close to continuum, whereas for $\ell > 1$ we are projected into the opposite, anticontinuum, domain with a transition zone around $\ell = 1$ which narrows as p increases.

In what follows we further explore the anticontinuum regime as $\varepsilon = 1/\ell^{p+1} \downarrow 0$. Since, as a by-product of genuine anharmonicity, the tails of solitary waves decay at superexponential rate, we shall consider a setup where all mass points beyond the first three may be assumed to vanish. Let $y_0(t)$ be the central point with the adjacent ones $y_{-1}(t)$ and $y_{+1}(t)$ symmetrically located around y_0 and thus $y_{-n}(t) = y_{+n}(t)$ at all times. We shall assume that $\cdots y_{\pm 2} \ll y_{\pm 1} \ll y_0$. The first

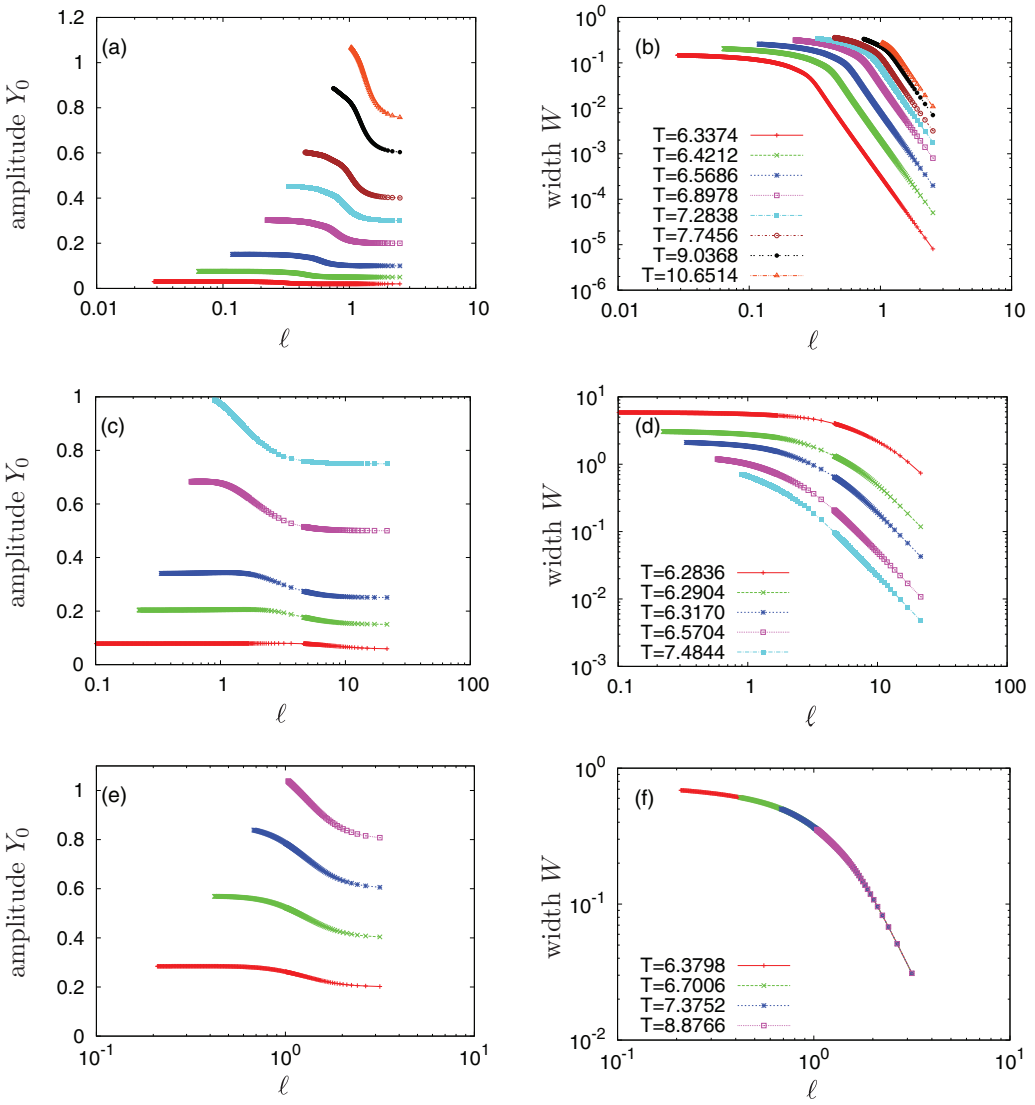

FIG. 3. (Color online) Dependence of the amplitude Y_0 and the width of breathers on the parameter ℓ, for different periods of the breathers, as depicted in width panels. (a, b) $m = 2, p = 4$; (c, d) $m = 4, p = 2$; (e, f) $m = p = 3$.

two chain equations of (3) thus read

$$\ddot{y}_0 + y_0 - y_0|y_0|^{m-1} = \varepsilon[(y_1 - y_0)|y_1 - y_0|^{p-1} - (y_0 - y_1)|y_0 - y_1|^{p-1}] \quad (19)$$

and

$$\ddot{y}_1 + y_1 - y_1|y_1|^{m-1} = \varepsilon[(-y_1)|-y_1|^{p-1} - (y_1 - y_0)|y_1 - y_0|^{p-1}], \quad (20)$$

with $y_{\pm 2}$ assumed to be negligible. Exploiting obvious antisymmetry and order relations we approximate our system as

$$\ddot{y}_0 + y_0 - y_0|y_0|^{m-1} + 2\varepsilon y_0|y_0|^{p-1} = 2p\varepsilon|y_0|^{p-1}y_1 + \cdots \quad (21)$$

and

$$\ddot{y}_1 + y_1 - y_1|y_1|^m = \varepsilon y_0|y_0|^{p-1} + \varepsilon p y_1|y_0|^{p-1} + \cdots . \quad (22)$$

It is obvious from (22) that $y_1 = O(\varepsilon y_0^p)$. To a leading order it can be thus further simplified:

$$\ddot{y}_1 + y_1 = \varepsilon y_0|y_0|^{p-1} \Rightarrow$$
$$y_1 = \varepsilon p \int_0^t \sin(t - r) y_0|y_0|^{p-1}(r)\, dr. \quad (23)$$

Further nodal points down the chain are similarly estimated; $y_2 = O(\varepsilon|y_1|^p)$ and $y_n = O(\varepsilon^{a_n}|y_0|^{np})$, $a_n = \sum_1^n p^j$, which reveals their exceedingly fast decay. In fact, to a leading order the dynamics of each such term is given by a linear response similar to that of y_1:

$$y_n = \varepsilon p \int_0^t \sin(t - r) y_{n-1}|y_{n-1}|^{p-1}(r)\, dr, \quad n \geqslant 1.$$

Returning to the leading Eq. (21) we note that the change due to y_1 is $O(\varepsilon^2)$ and to a leading order may be ignored. Integrating once we have $\frac{1}{2}\dot{y}_0^2 + P = P_0$ where $P = \frac{1}{2}y_0^2 - \frac{1}{1+m}|y_0|^{1+m} + \frac{2\varepsilon}{1+p}|y_0|^{1+p}$, with the interaction having only a minor impact on the effective potential, the maximal amplitude of oscillations

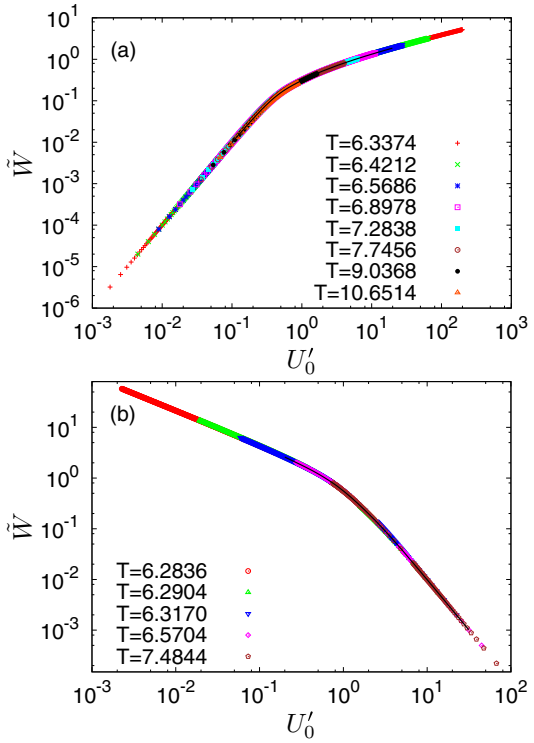

FIG. 4. (Color online) Breathers in lattice (17) (black line, almost indistinguishable from symbols). (a) $m = 2, p = 4$; (b) $m = 4, p = 2$. The symbols show rescaled data from the breathers in the D-QLKG lattices.

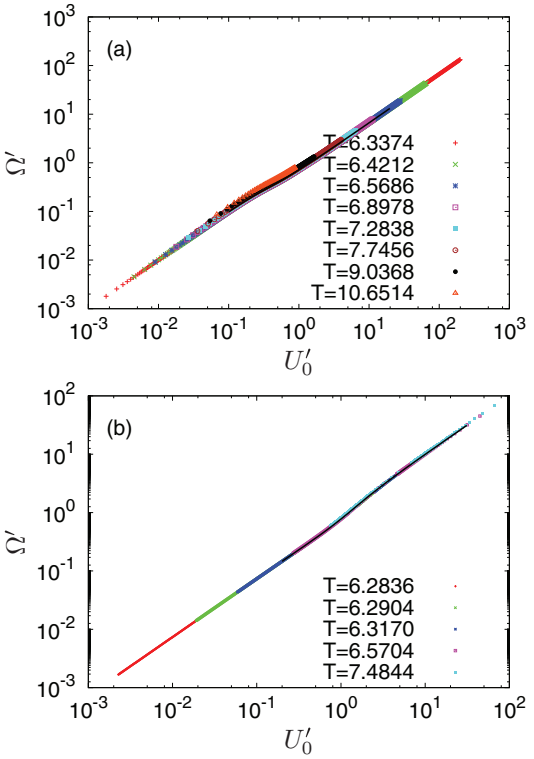

FIG. 5. (Color online) Breathers in lattice (17) (black line, almost indistinguishable from symbols). (a) $m = 2, p = 4$; (b) $m = 4, p = 2$. The symbols show rescaled data from the breathers in the D-QLKG lattices.

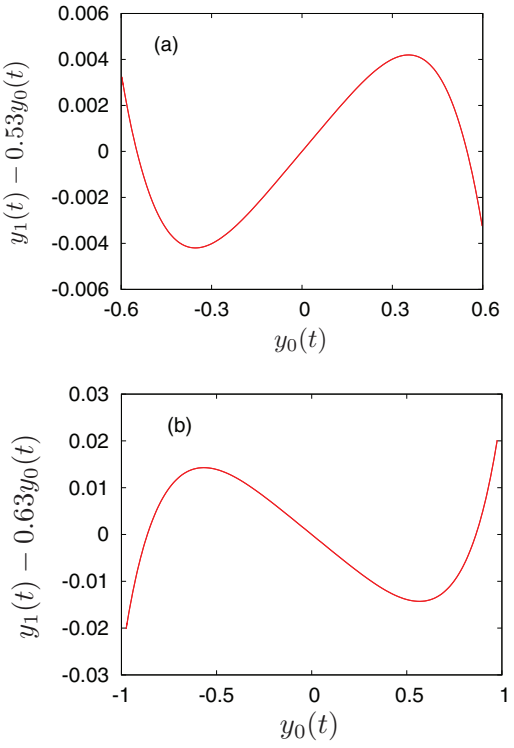

FIG. 6. (Color online) Test of time-space nonseparability of the D-QLKG breathers. (a) $m = 2, p = 4$. Period $T = 7.7456$, $\ell = 0.5060098, y_0 = 0.5980614$. (b) $m = 4, p = 2$. Period $T = 7.4844$, $\ell = 0.9950531, y_0 = 0.9752348$.

being now $y_{\max} = 1 + \frac{2\varepsilon}{m-1}$. Thus in the anticontinuum limit the breather has the lowest amplitude. In fact, in the separable $m = p = 3$ case $y_{\max} = \frac{1}{\sqrt{1-2\varepsilon}}$, whereas the continuum yields $y = \sqrt{2}$.

We now comment on restricting our discussion to site potentials with soft nonlinearity. From (21) one notes that the frequency at the central site y_0 (being the the frequency of the breather) is smaller than the one for soft nonlinearity and small ε. This implies that in the driven linear equation (22) the response y_1 is in phase with the driving mode y_0^p, and thus the amplitude of the breather does not change sign. As this property persists for large ε as well, where the simplified theory just presented is no longer valid, it is possible to construct breathers from the anticontinuum up to the continuum. For hard nonlinearity the situation is markedly different: now the frequency of the central site is larger than one, and oscillations of y_1 are in antiphase with y_0. The breather solution now takes a zigzagging form and thus cannot extend to up the continuum. In Sec. VII we shall present a class of such solutions.

V. IMPACT OF LINEAR INTERACTION

The purpose of this section is to see what structural changes are caused by retaining a small but finite linear interaction. To this end we derive a quasilinear Schrodinger approximation (QLS) for the coupling potential which includes linear interaction as well:

$$P(S) = \frac{a_1}{2}S^2 + \frac{a_p}{p+1}|S|^{p+1}, \tag{24}$$

where a_i are constants. The resulting equation in the continuum limit is then

$$y_{tt} + y = \frac{\partial}{\partial x}\{a_1 y_x + a_p y_x |y_x|^{p-1}\} + \Phi_1'(y). \qquad (25)$$

For $a_1 = 1, a_p = 0$, and $\Phi_1(y) = 1 - \cos y$ one recovers the sine-Gordon case, while for $a_1 = 0, a_3 = 1$, and $p = m = 3$ we are back at Eq. (4).

Applying the same averaging procedure on the original Newtonian lattice that yielded Eq. (5), we obtain this equation appended with the linear interaction:

$$-i\frac{dw_n}{dt} = \frac{1}{\ell}[T_n \nabla_n - T_{n-1}\nabla_{n-1}] + |w_n|^{m-1} w_n, \qquad (26)$$

where $T_n = \epsilon^2 + |\nabla_n|^{p-1}$, $\nabla_n = (w_{n+1} - w_n)/\ell$. Repeating the averaging procedure for the continuum version Eq. (25) and keeping only the leading term $b_m y^m$ in $\Phi_1'(y)$ we obtain

$$i w_t = \frac{\partial}{\partial x}[(d_1 + d_p |w_x|^{p-1}) w_x] + d_m |w|^{m-1} w, \qquad (27)$$

where $d_l = a_1/2$, $d_p = a_p/C_p$, $d_m = b_m/C_m$, and the coefficients C_l are the same as above. To keep both the harmonic and the anharmonic parts of the interaction while carrying the averaging procedure one assumes that both are on equal footing, which, for instance, for $p = 3$ would imply that $d_1 \sim |y_x|^2$. Equation (27) also admits harmonic vibrations: $w = \exp(i\omega t)U(x)$ with the spatial part in normalized units given via

$$[\epsilon^2 U' + U'|U'|^{p-1}]' + U|U|^{m-1} = U. \qquad (28)$$

Integrating once,

$$\epsilon^2 (U')^2 + \frac{2p}{p+1}|U'|^{p+1} + \frac{2}{m+1}|U|^{m+1} = U^2, \qquad (29)$$

with the integration constant discarded to ensure solitary solutions.

We now discuss the properties of the localized solutions. Assume in Eq. (29) that $p = 3$ and solve it in U'^2:

$$3(U')^2 = -\epsilon^2 + \sqrt{\epsilon^4 + 3\left(2U^2 - \frac{4|U|^{m+1}}{m+1}\right)}. \qquad (30)$$

The effect of finite sonic velocity is expressed by ϵ, and though its neglect has no singular effect on the equation, it does affect

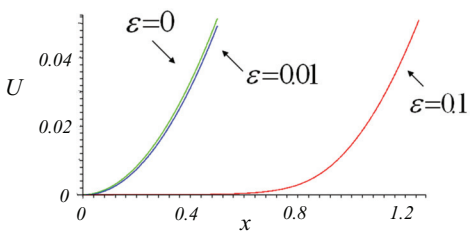

FIG. 7. (Color online) Tails of two solitary waves in close to compacton conditions and edge of a genuine compact breather. Note that the $\epsilon = 0.01$ and $\epsilon = 0$ cases, for all practical purposes, are indistinguishable.

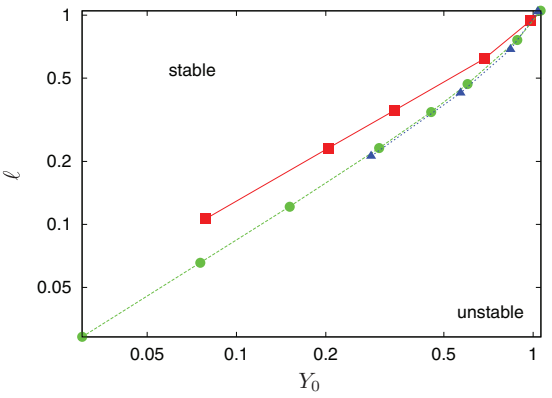

FIG. 8. (Color online) Stability regions for breathers in the D-QLKG. Green circles: $m = 2, p = 4$; blue triangles: $m = 3, p = 3$; red squares: $m = 4, p = 2$.

the solution near the tail and its top where for small ϵ: $U_{\max} \sim \sqrt{2}\{1 + \epsilon^4/12\}$. To see its impact on the tail, we neglect the last term in Eq. (30) and normalize

$$\frac{\epsilon^2}{2}(z')^2 = -1 + \sqrt{1 + z^2} \quad \text{where} \quad U = \frac{\epsilon^2}{\sqrt{6}} z, \qquad (31)$$

which for $z \ll \epsilon^2$ to a leading order yields $U \sim \epsilon^2 \exp x/\epsilon$. When $1 \ll z \ll 1/\epsilon^2$ expanding the radical in Eq. (31) we obtain $U = x^2/\sqrt{6} + O(\epsilon^2)$, which is the tail of the compacton. Thus for a small ϵ there is a boundary layer tail (Fig. 7) which collapses as $\epsilon \downarrow 0$.

VI. STABILITY OF BREATHERS

To study breathers' stability we have calculated the eigenvalues of the linearized equations in the D-QLS case and the multipliers of the found periodic orbit in the general D-QLKG case. Although breathers in D-QLKG and D-QLS have a similar shape, *their stability is markedly different*. Whereas the D-QLS breathers appear to be stable for all values of the studied parameters, the stability of the D-QLKG breathers strongly depends on the spareness parameter ℓ. Close to the anticontinuum limit the D-QLKG breathers are stable, but they become unstable at some finite ℓ as we march toward the continuous limit. In fact, in Fig. 3 the value at the left edge of each curve corresponds to a stability-wise extremal value of ℓ, as we stopped the continuation procedure of finding breathers when the absolute value of the largest in absolute value multiplier exceeded a threshold of $\approx$1.1.

In Fig. 8 domains of stability on the (ℓ, Y_0) plane are displayed. Observe that breathers on sparse lattices maintain their stability up to large amplitudes, whereas breathers on dense lattices are stable only at small amplitudes. This is similar to the results found for the separable $m = p = 3$ case; see Ref. [6]. Notably, in all studied cases we observe the stability threshold to follow a power law $\ell \sim Y_0^\beta$ with β close to one.

VII. ZIGZAGGONS: ALTERNATING SIGN BREATHERS

One of the tenets of the presented breathers is their macroscopic width, which with mild changes persists into

the continuum. Here we pause to present another class of breathers whose amplitude zigzags from site to site and thus are essentially microscopic modes without continuum extension. To this end we first limit the site potential to a quadratic form and in Eq. (2) set $b_m = 0$, i.e., $\Phi(y) = y^2/2$. Obviously, space-time separability $y_n = \phi(t)Y_n$ stays intact, yielding Eq. (7) for the temporal evolution of $\phi(t)$, whereas for Y_n we have again Eq. (15) but without the Y_n^m part. Introducing bond variable u_n (cf. Refs. [16,17]) we recast our system

$$\lambda u_n = \nabla_D^2(u_n|u_n|^{p-1}) \quad \text{where} \quad u_n \doteq \frac{1}{\ell}(Y_{n+1} - Y_n) \tag{32}$$

and $\nabla_D^2 A_n \doteq \{A_{n+1} - 2A_n + A_{n-1}\}/\ell^2$.

To derive the zigzagging breathers let $u_n = (-1)^n V_n$ and set $\lambda = -1$ (only the sign of λ matters). Thus, unlike previous cases, Eq. (7) now supports anharmonic oscillations of arbitrary amplitude. Thus

$$\nabla_D^2(V_n|V_n|^{p-1}) + \frac{4}{\ell^2}V_n|V_n|^{p-1} - V_n = 0. \tag{33}$$

In terms of the new variables we have an additional site force $4V_n^p/\ell^2$ that generates a potential well which supports localized structures. In our context they form an outer envelope of the zigzagging breather. To unfold their shape replace $\nabla_D^2 A_n$ with A_{xx}, its continuum limit, and $V_n \to V(x)$. The resulting equation

$$(V|V|^{p-1})'' + \frac{4}{\ell^2}V|V|^{p-1} - V = 0 \tag{34}$$

is recognized as $K(p,p)$ [18], which supports compactons

$$V(x) = (\pm 1)^p \left\{ \frac{p\ell^2}{2(1+p)} \cos^2\left[\frac{p-1}{p}\left(\frac{x}{\ell}\right)\right]\right\}^{\frac{1}{p-1}} \tag{35}$$

for $|[\cdots]| \leqslant \pi/2$ and vanishes elsewhere. Thus

$$V_n = V(n\ell) \quad \text{or} \quad V_n = V\left[\left(n + \frac{1}{2}\right)\ell\right].$$

The presence of spareness parameter ℓ implies that (35) describes an intrinsic mode which vanishes in the continuum limit. A direct comparison of (35) with a direct numerical solution of Eq. (32) (Fig. 9) shows (35) to be a good approximation. Notably, for the $p = 3$ solution Eq. (35) hints that Eq. (33) may also admit an exact periodic solution. In fact, we have

$$V_n = \pm\ell\sqrt{\frac{3}{8}}\cos\left(\frac{2n}{3}\right). \tag{36}$$

However, unlike the continuum case, the discrete wave does not have a critical amplitude at which it turns into a train of compactons; nevertheless it clearly indicates the viability of the continuum approximation (35) everywhere but at the edges where compactons' sharp cutoff is replaced by a doubly exponential decay.

Finally, using Eqs. (15) and (32) we express the breather in terms of the original variable

$$Y_n = (-1)^n[V_n|V_n|^{p-1} + V_{n-1}|V_{n-1}|^{p-1}]\ell^{-1}$$

and $y_n = \phi(t)Y_n$. Note that as elsewhere in this paper one may derive a small amplitude version with spatial shape of the resulting D-QLS breathers being exactly the same as in (34). Being harmonic, at large amplitudes they oscillate at a slower pace than the oscillations of the full problem.

It is natural to inquest whether the presented zigzaggons can exist in a lattice with nonlinear on-site potential (2). Unfortunately, extension of numerical methods of Sec. IV A is far from straightforward, as in the anticontinuum the solution is not a single-site oscillation. Instead, noting in Fig. 9(b) a very fast decay of the strongly nonlinear asymmetric sparse zigzaggons, in a similar fashion so Sec. IV B, we analyze the problem in the sparse lattice limit and construct a four-points antisymmetric compact breather. To this end we assume that $y_{1-n} = -y_n$, for $n \geqslant 1$. Then, the first two Eq. (3) read

$$\begin{aligned} \ddot{y}_1 + y_1 - y_1|y_1|^{m-1} &= \varepsilon[(y_2 - y_1)|y_2 - y_1|^{p-1} \\ &\quad - (2y_1)|2y_1|^{p-1}], \\ \ddot{y}_2 + y_2 - y_2|y_2|^{m-1} &= \varepsilon[(y_3 - y_2)|y_3 - y_2|^{p-1} \\ &\quad + (y_2 - y_1)|y_2 - y_1|^{p-1}]. \end{aligned} \tag{37}$$

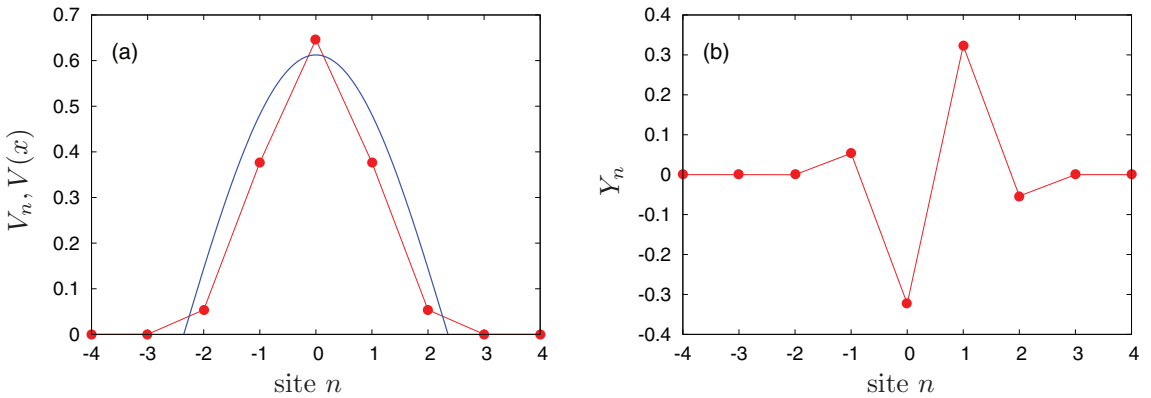

FIG. 9. (Color online) Solutions of Eqs. (33) (red markers) and (36) (blue line) (a), and the corresponding profile Y_n (b). Parameters $p = 3$, $\ell = 1$.

Assuming that $|y_2| \ll |y_1|$ and in particular that y_3 is negligible, we have

$$\ddot{y}_1 + y_1 - y_1|y_1|^{m-1} + 2^p \varepsilon y_1|y_1|^{p-1} = -\varepsilon p y_2|y_1|^{p-1} + \cdots, \tag{38}$$

$$\ddot{y}_2 + y_2 - \varepsilon y_1|y_1|^{p-1} = y_2|y_2|^{m-1} + \varepsilon p y_2|y_1|^{p-1} + \cdots. \tag{39}$$

Neglecting in the first approximation the terms on the right-hand side of Eqs. (38) and (39), we have a semicoupled system with y_1 driving the enslaved linear mode y_2 in (39). Similar relations hold between subsequent nodal points: the nth node drives the $(n+1)$ node, and so on. Depending on the sign of the local nonlinearity, b_m, the relation between m and p and the sparseness ε, the frequency of the nonlinear oscillator (38) may be larger or smaller then one. Correspondingly, two types of zigzagging breathers are possible: either the amplitudes y_n alternate in sign $\sim(-1)^n$, or, if the frequency is smaller than one, the amplitudes y_n have the same sign and the only sign change occurs between the central nodes y_0 and y_1.

VIII. DISCUSSION

In this paper we have presented breather solutions in a genuinely anharmonic one-dimensional Klein-Gordon lattices (D-QLKG) imbedded in a local site potential. Together with the basic model we have derived and studied a small, albeit finite, amplitude version with the fast oscillations averaged out. Though the resulting quasilinear Schrödinger lattice (D-QLS) and the continuum QLS equation are of independent mathematical and physical interest, their main role in the present context was to provide an insight into the breathers of the original Klein-Gordon lattice, where, unless close to the anticontinuum limit, we are totally at the mercy of numerics. Therefore attention was given to determine the utility of our small amplitude model renditions. In particular, we aimed to determine to what extent D-QLS breathers are a useful approximation of the original problem in terms of shape and stability. As the scalings presented in Figs. 4 and 5 indicate, the amplitude-frequency and amplitude-width dependencies of the original breathers are almost perfectly captured by their D-QLS rendition. But whereas the D-QLS breathers are unconditionally stable, the D-QLKG breathers become unstable at a sufficiently large amplitude, with the critical amplitude decreasing in tandem with the sparseness of the lattice, which plays a key role in stabilization of breathers. As a further indication of the close affinity between the original problem and its small amplitude rendition, we note that though in principle unless $m = p$ the space-time separability property is lost, in practice dynamics of breathers remains close to a separable state. Since for small ℓ stability suppresses the permissible amplitude (recall that stability threshold decreases with the spareness of the lattice) in this regime the D-QLS may suffice to describe breathers dynamics. Their harmonic oscillation implies space-time separability for all p and m in tandem with our numerical findings.

The strongly anharmonic lattice at already moderately large spareness parameter ℓ induces dynamics typical of an anticontinuum regime with breathers' motion confined to a very small number of participants. In fact, with a grain of salt one could say that our system is in either a continuum or anticontinuum phase separated in the vicinity of $\ell \sim 1$ by a narrow transition zone where discrete effects neither dominate nor are negligible.

Two topics are worth commenting on. First, the form of the studied nonlinearities: Clearly, since insofar that two different site potentials share the same first two terms in Taylor expansion, their averaging yields the same equation; therefore a given D-QLS, or QLS, is a generic small amplitude representation of a whole family of site potentials. This in turn implies that whereas small-amplitude features are generic, the large amplitude patterns generated by the D-QLKG-type equations may be model specific. Nevertheless, the maximal simplicity of the presented class of anharmonic Klein-Gordon lattices grants them a canonical status.

Second, several issues were left for future consideration. Among those we mention the impact of nonlinearities on a *waiting time* of a compact initial disturbances and dynamics of higher dimensional breathers. In particular, one may be interested in multinodal excitations similar to the ones presented in Ref. [15]. Note that, as we discussed in Ref. [6], in higher dimensions the transition to an isotropic continuum is limited to hexagonal lattices and $p \leqslant 3$.

ACKNOWLEDGMENTS

The research of P.R. was supported in part by the The Bauer-Neuman Chair in Applied Mathematics and Theoretical Mechanics. He also thanks IRTG 1740/TRP 2011/50151-0, funded by the DFG/FAPESP, for partial support.

[1] D. Campbell, S. Flach, and Y. Kivshar, Phys. Today **57**(1), 43 (2004).
[2] S. Aubry, Physica D **103**, 201 (1997).
[3] S. Flach and C. R. Willis, Phys. Rep. **295**, 181 (1998).
[4] S. Flach and A. V. Gorbach, Phys. Rep. **467**, 1 (2008).
[5] G. James, P. G. Kevrekidis, and J. Cuevas, Physica D **251**, 39 (2013).
[6] P. Rosenau and S. Schochet, Phys. Rev. Lett. **94**, 045503 (2005); Chaos **15**, 015111 (2005).
[7] P. Tchofo Dinda and M. Remoissenet, Phys. Rev. E **60**, 6218 (1999).
[8] M. Eleftheriou, B. Dey, and G. P. Tsironis, Phys. Rev. E **62**, 7540 (2000).
[9] B. Dey, M. Eleftheriou, S. Flach, and G. P. Tsironis, Phys. Rev. E **65**, 017601 (2001).
[10] J. C. Comte, Phys. Rev. E **65**, 067601 (2002).
[11] A. V. Gorbach and S. Flach, Phys. Rev. E **72**, 056607 (2005).
[12] K. Yoshimura, J. Math. Phys. **53**, 102701 (2012).
[13] G. James, Math. Mod. Methods Appl. Sci. **21**, 2335 (2011).
[14] J. A. Sanders and F. Verhulst, *Averaging Methods in Nonlinear Dynamical Systems* (Springer, Berlin, 1985).
[15] P. Rosenau, Phys. Lett. A **374**, 1663 (2010).
[16] P. Rosenau, Phys. Lett. A **118**, 222 (1986).
[17] P. Rosenau and A. Pikovsky, Phys. Rev. Lett. **94**, 174102 (2005).
[18] P. Rosenau and J. M. Hyman, Phys. Rev. Lett. **70**, 564 (1993).